Mechanisms of AAV2 neutralization by human alpha-defensins

Short Title: AAV neutralization by human alpha-defensins

Jessica M. Porter[a], Mackenzi S. Oswald[a], Kevin Busuttil[b], Shanan N. Emmanuel[b], Antonette Bennett[b], Robert McKenna[b], and Jason G. Smith[a,#]

[a]Department of Microbiology, University of Washington School of Medicine, Seattle, Washington, USA

[b]Department of Biochemistry and Molecular Biology, University of Florida College of Medicine, Gainesville, Florida, USA

[#]Address correspondence to Jason G. Smith, jgsmith2@uw.edu

Abstract

Antiviral immunity compromises the efficacy of adeno-associated virus (AAV) vectors used for gene therapy. This is well understood for the adaptive immune response. However, innate immune effectors like alpha-defensin antimicrobial peptides also block AAV infection, although their mechanisms of action are unknown. To address this gap in knowledge, we investigated AAV2 neutralization by human neutrophil peptide 1 (HNP1), a myeloid alpha-defensin, and human defensin 5 (HD5), an enteric alpha-defensin. We found that both defensins bind to AAV2 and inhibit infection at low micromolar concentrations. While HD5 prevents AAV2 from binding to cells, HNP1 does not. However, AAV2 exposed to HD5 after binding to cells is still neutralized, indicating an additional block to infection. Accordingly, both HD5 and HNP1 inhibit externalization of the VP1 unique domain, which contains a phospholipase A_2 enzyme required for endosome escape and nuclear localization signals required for nuclear entry. Consequently, both defensins prevent AAV2 from reaching the nucleus. Disruption of intracellular trafficking of the viral genome to the nucleus is reminiscent of how alpha-defensins neutralize other non-enveloped viruses, suggesting a common mechanism of inhibition. These results will inform the development of vectors capable of overcoming these hurdles to improve the efficiency of gene therapy.

Author Summary

AAVs are commonly used as gene therapy vectors due to their broad tropism and lack of disease association; however, host innate immune factors, such as human alpha-defensin antimicrobial peptides, can hinder gene delivery. Although it is becoming increasingly evident that human alpha-defensins can block infection by a wide range of nonenveloped viruses, including AAVs, their mechanism of action remains poorly understood. In this study, we describe for the first time how two types of abundant human alpha-defensins neutralize a specific AAV serotype, AAV2. We found that one defensin prevents AAV2 from binding to cells, the first step in infection, while both defensins block a critical later step in AAV2 entry. Our findings support the emerging idea that defensins use a common strategy to block infection by DNA viruses that replicate in the nucleus. Through understanding how innate immune effectors interact with and impede AAV infection, vectors can be developed to bypass these interventions and allow more efficient gene delivery.

Introduction

Adeno-associated virus (AAV) is a non-enveloped single-stranded DNA virus that belongs to the genus *Dependoparvovirus* of the *Parvoviridae* family. Their small icosahedral T=1 capsid is comprised of three viral capsid proteins, VP1, VP2, and VP3, which assemble stochastically in an approximately 1:1:10 ratio [1, 2]. There are currently 13 known AAV serotypes which were isolated from both human and non-human primate species [3-5]. Due to their diverse tropism and inability to replicate independently, recombinant AAVs (rAAVs) are used as gene therapy vectors [6-8]. There are currently seven approved rAAV-based gene therapies, with more being tested in clinical trials [8]. However, poor transduction efficiency and interactions with the host immune system present hurdles that must be overcome to produce more efficient vectors [6, 7, 9, 10]. While the interactions of AAVs with components of the adaptive immune response such as anti-capsid neutralizing antibodies [11-13] and T cells [14, 15] have been previously investigated, the interactions of AAVs with innate immune effectors including antimicrobial peptides such as human α-defensins are vastly understudied.

Defensins are short, amphipathic, and cationic innate immune peptides that have been studied for their antimicrobial properties [16, 17]. They are broadly antimicrobial against bacteria and fungi as well as enveloped and non-enveloped viruses. Their structures consist primarily of β-sheets stabilized by three disulfide bonds [16, 18, 19]. Some defensins also form dimers, which are essential for their antiviral activity [20-23]. There are two types of defensins produced by humans, α- and β-defensins. Human α-defensins can be further categorized into two subtypes: enteric and myeloid. Enteric α-defensins, human defensin 5 and 6 (HD5 and HD6), are constitutively secreted by Paneth cells in the crypts of the small intestine but are also present in the genitourinary tract [24, 25]. Myeloid α-defensins, human neutrophil peptides 1 to 4 (HNP1 to HNP4), are primarily expressed in neutrophils, where they are stored in cytoplasmic azurophilic granules that fuse with phagolysosomes following uptake of bacteria and viruses [16, 17, 19]. In

74 addition, neutrophils release HNPs into the extracellular space during the formation of neutrophil
75 extracellular traps [26].

76 While both α- and β-defensins have been shown to have activity against bacteria and
77 enveloped viruses, only α-defensins inhibit non-enveloped viral infection [18, 19]. Human
78 adenovirus (HAdV), human papilloma virus (HPV), polyoma virus, and rotavirus (RV) have all
79 been shown to be sensitive to neutralization by either HD5, HNP1, or both [27-34]. Previously,
80 Virella-Lowell and colleagues found that AAV2 can be inhibited by HNPs present in
81 bronchoalveolar fluid and by a mixture of purified HNP1 and HNP2 [35]. We recently showed that
82 AAV1 and AAV6 are also neutralized by HNP1 as well as HD5 [22]. In our previous studies with
83 HAdV and HPV, we found that α-defensins perturb viral uncoating, therefore preventing
84 productive infection [27, 29, 30, 36, 37]. A similar mechanism was determined for John
85 Cunningham (JC) polyomavirus neutralization by HD5 [33]. These findings suggest the possibility
86 of a common mechanism utilized by defensins to block non-enveloped viral infection. However,
87 alternative mechanisms of neutralization have also been described for polyomaviruses [32], and
88 the molecular basis for defensin-mediated inhibition of parvoviruses and rotaviruses has not been
89 elucidated.

90 To begin to determine how α-defensins inhibit AAV, we focused on AAV2. We found that
91 like the previously described effects of myeloid α-defensins HNP1 and HNP2 [35], the human
92 enteric α-defensin HD5 also neutralizes AAV2. We then sought to determine the stage of the
93 AAV2 cell entry pathway that is perturbed by each defensin. Although HD5 but not HNP1 could
94 inhibit AAV2 from binding to cells, both defensins were able to neutralize AAV2 when added post-
95 attachment, suggesting a common block at a downstream step. Consistent with this notion, we
96 found that both defensins inhibit the externalization of the unique domain of VP1 (VP1u), a crucial
97 step in AAV entry. This in turn prevents endosome escape and nuclear localization. Our findings
98 support the concept of a common mechanism by which human α-defensins neutralize non-

99 enveloped viruses by perturbing intracellular trafficking but also reveal a novel AAV-specific
100 mechanism.

101 **Results**

102 **Both HD5 and HNP1 bind to AAV2 and neutralize infection**

103 Prior studies have shown that human enteric and myeloid α-defensins may differentially
104 impact infection of non-enveloped viruses, including AAV1 [22, 27, 31, 33, 38]. Accordingly, we
105 first sought to determine the effects of HD5 and HNP1 on AAV2 infection using the same
106 physiologic defensin concentrations from our prior study [22]. When incubated with AAV2 on ice
107 before the mixture is added to cells (pre-attachment), both HD5 [inhibitory concentration (IC_{50}),
108 7.5 μM; 95% confidence interval (CI), 6.8 to 8.3 μM; Hill slope, -4.0] and HNP1 (IC_{50}, 9.7 μM; 95%
109 CI, <10.7 μM; Hill slope, -19.8) inhibit AAV2 infection with similar potency, and complete
110 neutralization is achieved by 40 μM HD5 and 20 μM HNP1 (Fig 1A and 1B). We then quantified
111 binding of each defensin to the AAV2 capsid by monitoring real-time kinetics of their interaction
112 using surface plasmon resonance (SPR). Consistent with our studies of AAV1 and AAV6 [22],
113 both defensins bind to the AAV2 capsid (Fig 1C and 1D). HNP1 [equilibrium dissociation constant
114 (K_D) = 0.32 ± 0.03 μM] bound with approximately 1.8-fold greater avidity than HD5 (K_D = 0.57 μM
115 ± 0.06 μM), while the stoichiometry of HD5 (385 ± 5 molecules per capsid) was approximately
116 1.7-fold greater than HNP1 (227 ± 10 molecules per capsid). Thus, in contrast to our prior findings
117 with AAV1 and AAV6 where both defensins bind to each serotype with similar avidity, HNP1 binds
118 more tightly than HD5 to AAV2. However, as was true for AAV1 and AAV6, more HD5 than HNP1
119 binds to AAV2.

120

121 **HD5, but not HNP1, inhibits AAV2 binding to cells**

122 To elucidate the mechanisms by which HD5 and HNP1 inhibit AAV2 infection, we first
123 determined if either defensin could block AAV2 from binding to cells. We used qPCR to enumerate

124 viral particles bound to the cell in the cold in the presence or absence of increasing concentrations
125 of defensin. HD5 (IC_{50}, 9.2 μM; 95% CI, 6.7 to 14.1 μM; Hill slope, -3.7), but not HNP1, inhibited
126 AAV2 cell binding (Fig 2A and B). Moreover, the IC_{50} of HD5 for binding (Fig 2A) and infection
127 (Fig 1A) are equivalent (P = 0.94), suggesting that disrupted binding is the primary mechanism
128 HD5 employs to block infection. We therefore reasoned that binding the virus to the cell prior to
129 defensin exposure might bypass inhibition of infection by HD5. However, contrary to our
130 expectations, HD5 still neutralized infection when added post-attachment (IC_{50}, 4.4 μM; 95% CI,
131 3.9 to 4.9 μM; Hill slope, -3.0) (Fig 2C). HNP1 also potently inhibited AAV2 under these conditions
132 (IC_{50}, 6.0 μM; 95% CI, 5.4 to 6.6 μM; Hill slope, -3.8), as expected (Fig 2D). Furthermore, as was
133 true for AAV6, both HD5 and HNP1 were more potent inhibitors of infection when added post-
134 attachment rather than pre-attachment (HD5, $P < 0.0001$; HNP1, $P = 0.0008$). Thus, while
135 inhibition of cell binding likely contributes to AAV2 neutralization by HD5, both defensins mediate
136 a block of infection downstream of binding.
137
138 **HD5 and HNP1 inhibit exposure of VP1u**
139 A critical post-binding step in AAV entry is endosome escape mediated by the
140 phospholipase A_2 (PLA2) domain of VP1u. Before AAV enters the cell, VP1u is held within the
141 capsid. However, conformational changes to the capsid occur within the endosome, resulting in
142 externalization of VP1u [39-43]. To determine if this conformational change is disrupted by
143 defensin interactions, we utilized antibodies [44] that bind either the externalized VP1u subunit
144 (A1) or an epitope on the external aspect of the VP3 domain (A20) in immunoprecipitation assays.
145 HeLa cells infected with AAV2 in the presence or absence of an inhibitory concentration of HD5
146 or HNP1 were harvested 6 h post-infection (p.i.), and virus was precipitated from cleared lysate
147 first by the A1 antibody then by the A20 antibody. Precipitated virus was visualized by immunoblot
148 using the B1 antibody against VP1, VP2, and VP3 [44, 45]. Because VP3 is more abundant
149 (approximately 10 VP3 to 1 VP1) and A1 binding to VP1u precipitates the entire capsid with which

150 it is associated, we quantified the ratio of VP3 in the A1 blots to VP3 in the A20 blots across
151 replicates. In the absence of defensin, both A1 and A20 bound AAV2 (Fig 3A-F). However, either
152 25 μM HD5 (Fig 3A and 3B) or 30 μM HNP1 (Fig 3C and 3D) was sufficient to block A1 binding,
153 suggesting the absence of accessible VP1u. These defensin concentrations also completely
154 inhibited infection under the conditions of this assay (Fig 3G-I). To exclude the possibility that the
155 lack of A1 binding or accessibility was due to defensins competing with A1 for its epitope in VP1u,
156 we infected cells in the absence of defensin, harvested at 6 h p.i., and then added HNP1 to the
157 cleared lysate prior to immunoprecipitation with A1 and A20. Under these conditions, both
158 antibodies reacted with AAV2 (Fig 3E and 3F), indicating that the defensins are unable to compete
159 with antibody binding. As an additional control, we utilized an HD5 analog (HD5abu) that is
160 incapable of forming disulfide bonds due to the substitution of α-aminobutyric acid for the six
161 cysteine residues in the linear sequence of HD5, rendering it non-functional as an antiviral (Fig
162 3G and 3I) [22]. HD5abu had no effect on A1 binding (Fig 3A and 3B), supporting the conclusion
163 that the lack of A1 reactivity in the presence of HD5 or HNP1 is due to a specific effect of the
164 defensins. From these experiments, we conclude that once the virus is internalized, both HD5
165 and HNP1 can prevent externalization of the VP1u subunit.
166
167 **Thermostability of the AAV2 capsid is not altered by either defensin**
168 During these experiments, we noticed the appearance of a weak, virus-specific band in
169 the A20-precipitated samples that was only present in the absence of defensin (arrows, Fig 4A
170 and 4B). Although it was not always observable in controls, likely due to the limit of detection of
171 the assay, it was always absent or noticeably reduced in defensin-treated samples. The mobility
172 of this band was faster than VP3, suggesting that it may be a proteolytic degradation product of
173 one or more capsid proteins that retains the B1 epitope. We have previously described such
174 degradation products of AAV2 capsids [46, 47]. The absence of this band in samples treated with
175 either HD5 or HNP1 suggested that the defensins may be stabilizing the capsid and preventing

176 proteolysis. To measure capsid stability more broadly, we utilized differential scanning fluorimetry
177 (DSF) in the presence or absence of either 25 μM HD5 or 30 μM HNP1 over a pH range from 4.0
178 to 7.4. This method uses the fluorescence of SYPRO Orange dye as a function of temperature to
179 determine the melting temperature (T_m) of the capsid. Although we observed a stabilizing effect
180 of pH, with a maximal T_m of 78.2°C at pH 5.5 compared to 66.4°C at pH 7.4 and 74.2°C at pH 4.0,
181 as observed previously [48], there was no effect of either defensin on thermostability (Fig 4C).
182 These results suggest that defensin binding to the capsid might block specific conformational
183 changes required for VP1u externalization or access of proteases to cleavage sites rather than
184 creating an overall more stable capsid.

185

186 **AAV2 fails to enter the nucleus and accumulates perinuclearly in the presence of defensins**

187 VP1u externalization serves at least two functions in AAV entry. The VP1u PLA2 domain
188 disrupts the endosomal membrane, and VP1u contains nuclear localization signals that facilitate
189 entry of the cytoplasmic capsid into the nucleus [40, 42, 49]. Therefore, we hypothesized that an
190 inability of AAV2 to externalize VP1u in the presence of defensins would manifest as a reduction
191 in nuclear localization of the capsid. We used confocal microscopy to visualize the trafficking of
192 AAV2 in the presence and absence of a neutralizing concentration of either HD5 or HNP1. In the
193 absence of defensin at 0 h p.i., DyLight 488 (DL488) AAV2 signal is diffuse with only coincidental
194 colocalization with the nuclear marker (DAPI) in z-projected images (Fig 5A-C), consistent with
195 the virus being bound to the outside of the cell. In contrast, at 24 h p.i., the viral signal is more
196 punctate, and pronounced nuclear localization was observed. In the presence of either HD5 or
197 HNP1 at inhibitory concentrations, AAV2 is punctate but exhibits markedly reduced nuclear
198 localization. Rather, the virus accumulates perinuclearly, which we quantified by measuring the
199 fraction of viral signal in each cell in a region spanning 5 pixels into and 50 pixels outside of the
200 nucleus (Fig 5D). In untreated samples, the perinuclear fraction is smaller than the nuclear

201 fraction; however, the ratio is reversed in HD5- or HNP1-treated samples (Fig 5E). Moreover, the
202 absolute intensity of AAV2 at 24 h p.i. in defensin-treated samples is higher than in untreated
203 samples (Fig 5F), which is consistent with reduced proteolytic degradation (Fig 4A and 4B). These
204 data, in combination with the lack of A1 reactivity described above, support a model whereby both
205 HD5 and HNP1 block VP1u externalization during entry, thereby impeding AAV2 from reaching
206 the nucleus and neutralizing infection.
207
208 **Discussion:**

209 In this study, we have demonstrated that AAV2 infection is neutralized by both enteric and
210 myeloid α-defensins with similar potency. In a normal infection, AAV2 binds to cells through
211 interactions with heparan sulfate proteoglycan attachment factors [50] and is endocytosed (Fig 6,
212 left). In the endosome, the VP1u subunit, which was kept within the capsid prior to entry, is
213 externalized [8, 39-42, 51]. This step is crucial for AAV2 entry, as the VP1u PLA2 domain
214 mediates breakdown of the endosomal membrane, allowing virions to escape into the cytosol
215 [43]. Host factors required for these steps are incompletely understood, but changes in pH and
216 interactions with recently identified proteinaceous host factors including KIAA0319L (AAVR) and
217 GPR108 play important roles [8, 51-55]. Once released from the endosome, the virus traffics
218 along microtubules, and nuclear localization signals in VP1 and VP2 mediate entry of the AAV2
219 virion into the nucleus [42, 49, 56-58]. The virion then uncoats in the nucleolus, releasing its
220 genome to begin transcription and replication [59, 60]. In the presence of defensins, two crucial
221 steps in this entry pathway are perturbed: cell binding and VP1u exposure (Fig 6, right). HD5 but
222 not HNP1 perturbs cell binding, if encountered by AAV2 prior to cell attachment. However, if AAV2
223 succeeds in binding to the cell and becomes internalized, HD5 and HNP1 both prevent the
224 externalization of the VP1u subunit, thereby trapping the virus in the endosome and blocking
225 cellular trafficking and nuclear entry.

226 How defensins interact with the capsid to block VP1u externalization remains unknown.
227 One model is that VP1u is externalized through channels at the 5-fold axes that are too small to
228 accommodate folded VP1u prior to conformational changes induced by the endosomal
229 environment [61, 62]. In addition to localized changes at the 5-fold vertices, more extensive
230 rearrangements involving other areas of the capsid including the 2-fold axis have been postulated
231 [61, 63]. Our data suggest that defensins do not increase the overall thermostability of the AAV2
232 capsid, arguing against a model where the entire capsid is stabilized against host-induced
233 conformational changes upon defensin binding. However, steric hinderance at the 5-fold axis pore
234 may prevent either the necessary local conformational changes from occurring or block VP1u
235 from threading through the pore. A similar model has been postulated for the anti-AAV8
236 and -AAV9 antibody HL2372 and the POROS CaptureSelect affinity ligand CSAL9, both of which
237 bind to the 5-fold axis and neutralize infection [64-66]. In our prior studies of differences in
238 defensin sensitivity of AAV1 and AAV6, the crucial residue was located at position 531 located on
239 the arm of the 3-fold protrusion extending along the wall of the 2-fold axis [22]. A positively
240 charged residue at this location (lysine) was associated with more uniform sensitivity to defensin
241 neutralization. In contrast, viruses bearing a negatively charged residue (glutamic acid) had
242 variable phenotypes dependent upon when defensin was added relative to cell binding. Therefore,
243 we hypothesized that amino acid 531 is not directly involved in binding to cationic defensins.
244 Rather, the nature of this residue may dictate surface charge at other parts of the capsid to
245 modulate defensin interactions. A hint to the location of defensin interactions with AAV2 may be
246 obtained by mapping the proteolytic cleavage site that appears to be blocked by both HD5 and
247 HNP1 binding. We have previously described such degradation products of AAV2 capsids at
248 endolysosomal pH [46, 47]. Although acidification of the capsid in the endolysosome has been
249 shown to be important for VP1u externalization and viral trafficking [39, 67, 68], the significance
250 of proteolysis of the AAV capsid at endolysosomal pH has not been elucidated, especially since
251 the capsid appears to be more stable at this pH. The residues predicted to be involved in AAV2

252 pH-induced proteolysis are located across the 2-fold axis along the wall of the 3-fold protrusion
253 near amino acid 531 [46]. However, even if we assume that AAV1 and AAV6 are neutralized by
254 the same mechanisms as AAV2, direct binding of defensin to these sites does not fully explain
255 the effect of defensin binding on VP1u externalization, unless there are structural conformations
256 at the 2-fold axis and 3-fold protrusion that indirectly affect the structure of the 5-fold axis and
257 ultimately prevent the externalization/accessibility of VP1u [63]. Definitive mechanistic insight
258 awaits structural information on the defensin-AAV2 complex.

259 Although both HD5 and HNP1 block VP1u externalization, their interactions with the
260 capsid differ. First, only HD5 disrupts AAV2 from binding to the cell. This mode of neutralization
261 by α-defensins is uncommon, having only been described previously for BK polyomavirus, where
262 HD5 aggregates the virus and reduces cell binding [32]. In contrast, cell binding of many viruses
263 like HAdVs, mouse AdV, and HIV-1 and is promoted by α-defensins [28, 36, 69-71]. Second,
264 HNP1 binds AAV2 more tightly than HD5 does, but there is less HNP1 than HD5 bound to the
265 capsid at equilibrium. These differences are not surprising given that the two defensins, although
266 structurally similar, vary in primary sequence, net charge, and charge distribution. Unlike
267 antibodies, defensins do not bind to a specific epitope. Rather, selective binding to favorable
268 capsid regions may initially occur over a range of affinities. Primary binding may then promote
269 additional defensin-defensin and defensin-capsid interactions. HD5, with weaker but more
270 abundant binding, may sterically occlude heparan sulfate proteoglycan (HSPG) binding sites,
271 inhibiting cell binding. HNP1 instead may bind preferentially to less abundant, higher affinity sites
272 away from the HSPG binding site, allowing cell binding to occur. Thus, it is reasonable to postulate
273 that the binding sites utilized by each defensin may not entirely overlap. These findings are
274 reminiscent of HPV interactions with defensins, where genital types differ in their sensitivities to
275 HD5 and HNP1 and where HD5 inhibits multiple steps of HPV16 entry [29-31].

276 By blocking the externalization of VP1u, the PLA_2 domain is unable to access the limiting
277 membrane, likely trapping the virus within the endosome. This interpretation is based on the
278 failure of defensin-treated virus to reach the nucleus; however, we did not measure endosomal
279 escape directly. It is plausible that defensins bound to the capsid could mediate endosome escape
280 through their ability to form pores in lipid bilayers [72]. In this case the absence of externalized
281 nuclear localization signals found in VP1u and the VP1/2 common region would still prevent the
282 virus from reaching and entering the nucleus [42, 49]. Thus, the increased amount of detectable
283 virus in defensin-treated samples at 24 h p.i. could be explained by defensin-induced viral
284 aggregation in either the endosome or cytoplasm, protection of virus trapped in the
285 endolysosomal system from lysosomal degradation, or protection of virus in the cytoplasm from
286 ubiquitination and proteosomal degradation. These mechanisms are not mutually exclusive,
287 although we note that all samples are treated with the proteosome inhibitor doxorubicin, which
288 has been shown to increase AAV transduction efficiency [73].

289 Without additional experimentation, it is difficult to anticipate the generalizability of our
290 findings to other AAV serotypes. Both AAV2 and AAV6 are neutralized by both HD5 and HNP1
291 when added to the virus either pre- or post-attachment to the cell [22]. However, the sensitivity of
292 AAV1 to each defensin depends on the order-of-addition, where HD5 is only neutralizing when
293 added pre-attachment and HNP1 is only neutralizing when added post-attachment. As described
294 above, the identity of residue 531 in VP3 solely dictates the defensin sensitivities of AAV1 and
295 AAV6. Although the defensin-dependent phenotypes of AAV2 and AAV6 are more similar, AAV2
296 and AAV1 (not AAV6) have the same residue (glutamic acid) at this position. Thus, the identity of
297 the residue at position 531 is not predictive. AAV2 and AAV6 share the ability to utilize HSPG as
298 an attachment factor [74], while AAV1 uses sialic acid [75]. Therefore, the nature of the
299 attachment factor might correlate with defensin sensitivity, particularly regarding blocking cell
300 binding. Until more serotypes are studied and a completely defensin-resistant serotype is

301 identified, it is hard to determine which characteristics might foretell defensin sensitivity; however,
302 our findings provide a blueprint for key assays that will inform neutralization mechanisms.

303 Finally, our findings may inform the development of AAV vectors. HNP levels are
304 increased in patients with highly inflammatory disease states, such as cystic fibrosis, which would
305 impair the delivery of gene therapy by defensin-sensitive serotypes such as AAV2 [35]. By
306 identifying where in the entry pathway innate immune peptides such as defensins inhibit, mutant
307 vectors can be better designed with the goal of escaping neutralization. Alternatively, existing
308 vectors that have been customized for tropism or antibody escape can be further tested for
309 defensin sensitivity [8]. Importantly, our findings provide two points of likely inhibition, cell binding
310 and endosome escape, that can be targeted in the development of escape variants.

311 **Materials and Methods**

312 **Cells.** HeLa (ATCC) and HEK293 cells (ATCC or University of Florida Powell Gene Therapy
313 Center Vector Core) were cultured in Dulbecco's modified Eagle's media (DMEM) supplemented
314 with 10% Fetal Bovine Serum (FBS), 0.1 mM non-essential amino acids, 4 mM L-glutamine, 100
315 units/mL penicillin, and 100 µg/mL streptomycin.

316 **Vector production and purification.**

317 The AAV2 vector expressing GFP was produced by triple transfection in mammalian HEK293
318 cells. HEK293 cells were cultured to approximately 80% confluency in 150 mm cell culture and
319 triple transfected with an equimolar ratio of pXRAAV2 [76], pTR-UF11-GFP [77], and pXX6
320 (pHelper) [78] plasmids (totaling 40 µg/plate), which were diluted with 1 mL Optimem (Gibco) and
321 125 µL of 1 mg/ml polyethyleneimine (PEI) per plate. The solution was incubated for 15 min at
322 RT and added dropwise to each plate. Cells were harvested 7 h post-transfection and separated
323 from the supernatant by centrifugation at 1100 × g in a JA-20 rotor at 4°C for 15 min. The cell
324 pellet was resuspended in TD buffer (1X PBS, 5 mM $MgCl_2$, 2.5 mM KCl, pH 7.4) and lysed by
325 three freeze/thaw cycles, followed by Benzonase (Promega) treatment at 37°C for 1 h. The
326 cellular debris was removed by centrifugation at 3000 × g, and the cell lysate was stored at -80°C.
327 The supernatant was PEG precipitated overnight with 10% (w/v) PEG 8000 (Fisher) and then
328 centrifuged at 14,300 × g in a JA-10 rotor at 4°C for 90 min. The resulting pellet was resuspended
329 in TD buffer and combined with the cell lysate, and AAV2 capsids were purified by AVB affinity
330 chromatography on a 1 mL AVB Sepharose affinity chromatography column (Cytvia,
331 Marlborough, MA), as previously described [74, 79]. Virus was eluted with 10 mL of elution buffer
332 (0.1 M glycine-HCl, pH 2.7) and neutralized with 1 mL of neutralization buffer (1 M Tris-HCl, pH
333 10.0). The final sample was concentrated and buffer exchanged using an Apollo concentrator
334 (Orbital Bioscience), and the purity was verified by SDS-PAGE.

335 Purified AAV2 at approximately 0.5 mg/mL was extensively dialyzed into PBS and labeled with
336 the DyLight Antibody Labeling Kit (Thermo Fischer) according to the manufacturer's protocol. The
337 completed reaction was dialyzed three times into PBS. Labeled virus was visualized by SDS-
338 PAGE using UV light to detect the fluorophore and quantified by Coomassie Blue staining against
339 BSA standards.

340 **α-defensin peptides.** HD5 (ATCYCRTHECATRESLSGVCEISGRLYRLCCR) and HNP1
341 (ACYCRIPACIAGERRYGTCIYQGRLWAFCC) were synthesized by CPC Scientific (Sunnyvale,
342 CA) and processed as previously described [34]. In brief, peptides were folded and stabilized by
343 thiol-disulfide reshuffling and purified by reverse-phase high-pressure liquid chromatography (RP-
344 HPLC) to homogeneity. Purity was analyzed by analytical RP-HPLC, verified by mass
345 spectrometry, and quantified by UV absorbance at 280 nm. HD5abu synthesis, purification, and
346 validation have been described previously [20, 21].

347 **Primary antibodies.** A1 (American Research Products, 03-61056) binds an epitope in VP1u [44,
348 45]. A20 (American Research Products, 03-61055) binds an epitope in the VP1/VP2/VP3
349 common domain of intact AAV2 [45]. B1 (University of Florida Hybridoma Core) binds an epitope
350 in the VP1/VP2/VP3 common domain of uncoated AAV2 [44, 45].

351 **Infection assays.** Infection assays were performed as previously described [22]. All viruses and
352 defensins were diluted in serum-free DMEM (SFM) supplemented with 1 μM doxorubicin (Dox).
353 AAV2 was diluted to 5.4E+10 viral genomes (vg)/mL for pre-attachment and 1.4E+11 vg/mL for
354 post-attachment. In brief, for pre-attachment exposure of AAV2 to defensins, 28 μL of AAV2 and
355 28 μL of SFM with or without HD5 or HNP1 were mixed and incubated on ice for 45 min before
356 50 μL of the mixture was added to cells. Samples were then incubated at 37°C. For post-
357 attachment exposure of AAV2 to defensins, 50 μL AAV2 was added to chilled cells and allowed
358 to bind for 1 h at 4°C. Samples were washed twice with ice-cold SFM before 50 μL SFM with or
359 without HD5 or HNP1 was added. Defensins were bound at 4°C for 45 min before cells were

360 moved to 37°C. For both conditions, 10 µL 60% FBS in SFM + 1 µM Dox was added to the wells
361 6 h p.i. At 48 h p.i., cells were washed with phosphate-buffered saline (PBS), and total monolayer
362 fluorescence was quantified with an Azure Sapphire. Background-subtracted total monolayer
363 fluorescence was further analyzed with Fiji (version 2.14.0/1.54f). Data are shown as the
364 percentage of control infection in the absence of defensin.

365 **SPR:** SPR experiments were performed on a BIAcore X100 instrument at 25°C, with PBS as the
366 running buffer, as previously described [22]. AAV2 was coupled to the CM5 sensor chip using
367 amine coupling, and 9451 response units (RUs) were immobilized. HD5 or HNP1 was the analyte,
368 and the same sensor chip was used for 2 replicate analyses on different days. Data were analyzed
369 as described previously to determine K_D, using the 1:1 binding model in BIAcore X100 evaluation
370 software (version 2.0.0), and stoichiometry, using GraphPad Prism (version 10.3.0).

371 **Cell binding assays:** HeLa cells were detached using 0.5 M EDTA, washed twice with cold SFM,
372 and resuspended in SFM + 0.2% sodium azide (SA). 8.4E+9 particles of AAV2 were incubated
373 with SFM + 0.2% SA with or without twice the final concentration of HD5 or HNP1 in a volume of
374 56 µL. Following incubation for 45 min on ice, 50 µL of the virus/defensin mixture was added to
375 5.0E+5 HeLa cells in a final volume of 100 µL. Samples were incubated for 90 min on ice with
376 intermittent agitation to allow binding. One sample without defensin was reserved as an input
377 control for quantitation. Remaining samples were washed three times with ice cold DMEM. All
378 samples were lysed and processed to extract genomic DNA using the Genejet Genomic DNA
379 Purification kit (Thermofisher) per the manufacturer's instructions. DNA was eluted from the
380 column in 100 µL elution buffer. qPCR was performed using SsoAdvanced SYBR Green master
381 mix (Bio-Rad) with primers for GFP (F: 5'-CCCAGACCATATGAAGCAGC-3'; R: 5'-
382 GCCCTTAGCTCGATTCTCT-3'). MOI bound was determined from a standard curve produced
383 by a dilution series of the input control. Note that diluting experimental samples 10-fold prior to

384 analysis was required for accurate quantitation. Data for each replicate were normalized to the
385 amount of virus bound in the absence of defensin.

386 **Immunoprecipitation and western blot:** HeLa cells were seeded at 6.0E+5 cells/mL in 6-well
387 plates and cultured overnight. Cells were infected with AAV2 at an MOI of 65,000 vg/cell in 1 mL
388 cold SFM. After incubation for 1 h at 4°C while rocking, the inoculum was removed and replaced
389 with 1 mL SFM with or without 25 μM HD5, 25 μM HD5abu, or 30 μM HNP1. After an additional
390 incubation for 45 min at 4°C while rocking, plates were shifted to 37°C for 6 h. Cells were washed
391 two times with ice cold PBS, scaped to detach them from the plate, and concentrated in chilled
392 1.5 mL Eppendorf tubes by centrifugation at 400 × g for 5 min at 4°C. The pellet was lysed in 100
393 μL immunoprecipitation (IP) buffer (20 mM Tris, 137 mM NaCl, 1% Triton X-100, 2 mM EDTA, 1X
394 HALT protease inhibitor, pH 8), freeze-thawed three times, and centrifuged at 25,000 × g for 10
395 min at 4°C. Anti-AAV VP1 (A1, 200 ng) was added to the clarified lysate, and samples were
396 incubated overnight at 4°C with constant agitation. A1-bound AAV2 was precipitated with Protein
397 G-PLUS agarose beads (Santa Cruz Biotech). Anti-AAV2 VP1/2/3 (A20) antibody (200 ng) was
398 then added to the supernatant. Samples were incubated for ≥ 3 h at 4°C with constant agitation
399 and precipitated with Protein G-PLUS agarose beads. For both precipitations, beads were
400 washed three times with IP buffer, and samples were eluted with SDS-loading buffer (3.2% SDS,
401 100 mM Tris, 0.04% bromophenol blue, 16% glycerol (w/v), 40 mM dithiothreitol, pH 6.8). Heat-
402 denatured (95°C for 5 min) samples were analyzed via SDS-PAGE on 10% polyacrylamide gels,
403 transferred to 0.45 μm nitrocellulose membranes, blocked for 1 h at RT in blocking buffer [3%
404 bovine serum albumin (BSA) and 1% Tween-20 in Tris-buffered saline (TBS): 20 mM Tris, 150
405 mM NaCl, pH 8.0]. Membranes were incubated with anti-AAV B1 antibody (333 ng/mL) in blocking
406 buffer at 4°C overnight, washed three times in TBS + 1% Tween-20, probed with goat anti-mouse
407 Alexa Fluor 488-conjugated secondary antibody (ThermoFisher, A-11001, 1:1000) in blocking
408 buffer, washed twice with TBS + 1% Tween-20 and once with TBS, and imaged on an Azure

409 Sapphire imager. Bands were quantified using AzureSpot Pro (v2.1.097). Data is the ratio of the
410 background subtracted volume of the A1 VP3 band divided by the A20 VP3 band for each sample.

411 **Differential Scanning Fluorimetry:** The stability of AAV2 was determined by differential
412 scanning fluorimetry (DSF) analysis using a Bio-Rad MyiQ2 Thermocycler to monitor the
413 fluorescence produced by the binding of SYPRO Orange dye (Invitrogen) to hydrophobic regions
414 of the AAV2 capsid upon heat denaturation. The temperature of the assay ranged from 30°C to
415 99°C, ramping at 0.5°C per step. Purified AAV2 (1 µg) was diluted in 22.5 µL of either 25 µM
416 HD5 or 30 µM HNP1 in citrate-phosphate (0.1 M citric acid, 0.2 M Na_2HPO_4) buffers at pH 7.4,
417 pH 6, pH 5.5, or pH 4. Samples were incubated for 30 min at RT before 2.5 µl/sample of 1%
418 SYPRO Orange dye was added. Samples containing buffer alone were used as negative
419 controls. Data is the inverse of the negative rate of change of relative fluorescence units vs
420 temperature (−dRFU/dT). The peak value on the resulting thermogram is the T_m. All experiments
421 were conducted in triplicate.

422 **Quantification of subcellular localization:** HeLa cells were cultured on glass coverslips
423 overnight. DyLight 488-labelled AAV2 in cold SFM containing 1 µM Dox at an MOI of 20,000
424 vg/cell was added, and cells were incubated for 1 h in the dark at 4°C. The inoculum was removed
425 and replaced with 50 µL SFM containing 1 µM Dox with or without 25 µM HD5 or 30 µM HNP1.
426 After incubation for 45 min at 4°C, one set of control coverslips was washed with PBS before
427 being fixed in 2% PFA (Electron Microscopy Science, 15710) for 15 min at RT. The remaining
428 cells were shifted to 37°C. At 6 h p.i., coverslips were moved to normal growth media, cultured
429 for an additional 18 h, washed with PBS, and fixed. Fixed cells were washed once with PBS and
430 incubated for 20 min at RT in permeabilization buffer (20 mM glycine, 0.5% Triton X-100, PBS).
431 Cells were sequentially stained with AF647-conjugated phalloidin (Abcam, ab176759, 1:1000) in
432 1% BSA, 0.05% Tween-80 in PBS for 45 min at RT then with 500 ng/mL DAPI for 5 min.
433 Coverslips were mounted with Prolong Gold (Life Technologies, P36930).

434 Z-series of images spanning entire cells were obtained using a confocal laser-scanning
435 microscope (Zeiss LSM 800) using a 63× objective. A maximum intensity z-projection of each
436 color channel for each field of view was generated using Fiji (v2.14.0/1.54h). Background
437 thresholds for AAV2 signal were determined manually for each replicate in Fiji using uninfected
438 negative controls. A human-in-the-loop model was trained in CellPose 2.0 [80] to identify cell
439 borders and generate cell masks. CellPose masks and z-projection images were imported into
440 CellProfiler (v4.2.5) [81], and background-subtracted single-cell images were identified and
441 exported. A second CellProfiler pipeline was then used to analyze the single-cell images. Nuclei
442 were identified using DAPI by thresholding using the Otsu method. A tertiary object extending 5
443 pixels into and 50 pixels beyond the nucleus was then defined as the perinuclear space, and the
444 integrated intensities of DyLight 488 within the whole cell, in the perinuclear space, and in the
445 nucleus were measured for each cell. Whole cells with DyLight 488 intensity < 100 relative
446 fluorescence units (RFU) were excluded from analysis.

447 **Statistical analysis:** All statistical analysis was performed with GraphPad Prism 10.3.0. Fig 1A,
448 1B, 2A, 2C, and 2D were analyzed by nonlinear regression using the "log (inhibitor) versus
449 response – variable slope (four parameters)" model with the bottom constrained to "0". Hill slopes
450 and IC_{50} values are the best-fit values. Log IC_{50} values were compared between protocol
451 conditions and assays (e.g., cell binding and inhibition of infection) using the extra-sum-of-
452 squares F test, and the P values are given. Fig 2B was analyzed by nonlinear regression using
453 the "log (agonist) versus response – variable slope (four parameters)" model with the bottom
454 constrained to "0". In Fig 3B and 3I for HD5 and HD5abu, repeated measures one-way ANOVA
455 using Dunnett's multiple comparisons test with a single pooled variance was used to compare the
456 mean of each column with that of the "no defensin" control. In Fig 3D, 3F, and 3I a two-tailed,
457 paired t test was used to compare HNP1 samples with "no defensin" controls. In Fig 3I, HD5 and
458 HD5abu were analyzed in parallel, while HNP1 was analyzed in separate experiments with

459 distinct “no defensin” controls. HD5, HD5abu, and HNP1 samples are graphed together for clarity.
460 Fig 4C was analyzed by repeated measures two-way ANOVA using Dunnett’s multiple
461 comparisons test with a single pooled variance to compare the mean of each column with that of
462 the “no defensin” control for each pH value. Fig 5A, 5B, 5E and 5F were analyzed by ordinary
463 one-way ANOVA using Dunnett’s multiple comparisons test with a single pooled variance to
464 compare the mean of each column with that of the “no defensin” control. In Fig 5A, each replicate
465 was analyzed individually. In Fig 5B, 5E, and 5F, the data for each condition for all replicates was
466 pooled prior to analysis. In Fig 5E and 5F, data was log-transformed prior to analysis. For all
467 analyses by ANOVA, P values are adjusted to account for multiple comparisons.

468

469 **Acknowledgements**

470 The authors would like to dedicate this study to the memory of Dr. Agbandje-McKenna, who was
471 a pioneer in the field of AAV structural biology. We thank Qun Tang and Melike Caglayan for
472 technical assistance with SPR experiments. We thank Dr. Matthew Parsek for the generous use
473 of his microscope and Dr. Jeffrey Carey and Dr. Xuhui Zheng in the Parsek lab for technical
474 assistance with microscopy. This work was supported by R01 AI104920 (to J.G.S. and R.M.),
475 from the National Institute of Allergy and Infectious Diseases (www.niaid.nih.gov) and by the
476 Office of the Director, National Institutes of Health (www.nih.gov/institutes-nih/nih-office-director)
477 under Award Number S10 OD026741 (to J.G.S.). Additional support to J.G.S. in the form of
478 subsidized core services was provided by NIH grants UL1 TR000423 from the National Center
479 for Advancing Translational Sciences (ncats.nih.gov), and P30 CA015704 from the National
480 Cancer Institute (www.cancer.gov). The funders had no role in study design, data collection and
481 analysis, decision to publish, or preparation of the manuscript.

482 **References:**

483 1. Meyer NL, Chapman MS. Adeno-associated virus (AAV) cell entry: structural insights. Trends
484 Microbiol. 2022;30(5):432-51. Epub 20211025. doi: 10.1016/j.tim.2021.09.005. PubMed PMID:
485 34711462.

486 2. Worner TP, Bennett A, Habka S, Snijder J, Friese O, Powers T, et al. Adeno-associated virus capsid
487 assembly is divergent and stochastic. Nature communications. 2021;12(1):1642. Epub 20210312.
488 doi: 10.1038/s41467-021-21935-5. PubMed PMID: 33712599; PubMed Central PMCID:
489 PMCPMC7955066.

490 3. Gao G, Vandenberghe LH, Alvira MR, Lu Y, Calcedo R, Zhou X, et al. Clades of Adeno-associated
491 viruses are widely disseminated in human tissues. J Virol. 2004;78(12):6381-8. Epub 2004/05/28.
492 doi: 10.1128/JVI.78.12.6381-6388.2004. PubMed PMID: 15163731; PubMed Central PMCID:
493 PMCPMC416542.

494 4. Schmidt M, Grot E, Cervenka P, Wainer S, Buck C, Chiorini JA. Identification and characterization of
495 novel adeno-associated virus isolates in ATCC virus stocks. J Virol. 2006;80(10):5082-5. doi:
496 10.1128/JVI.80.10.5082-5085.2006. PubMed PMID: 16641301; PubMed Central PMCID:
497 PMCPMC1472088.

498 5. Bossis I, Chiorini JA. Cloning of an avian adeno-associated virus (AAAV) and generation of
499 recombinant AAAV particles. J Virol. 2003;77(12):6799-810. doi: 10.1128/jvi.77.12.6799-6810.2003.
500 PubMed PMID: 12768000; PubMed Central PMCID: PMCPMC156192.

501 6. Large EE, Silveria MA, Zane GM, Weerakoon O, Chapman MS. Adeno-Associated Virus (AAV) Gene
502 Delivery: Dissecting Molecular Interactions upon Cell Entry. Viruses. 2021;13(7). Epub 20210710.
503 doi: 10.3390/v13071336. PubMed PMID: 34372542; PubMed Central PMCID: PMCPMC8310307.

504 7. Pillay S, Carette JE. Host determinants of adeno-associated viral vector entry. Curr Opin Virol.
505 2017;24:124-31. Epub 20170630. doi: 10.1016/j.coviro.2017.06.003. PubMed PMID: 28672171;
506 PubMed Central PMCID: PMCPMC5549665.
507 8. Lopez-Gordo E, Chamberlain K, Riyad JM, Kohlbrenner E, Weber T. Natural Adeno-Associated Virus
508 Serotypes and Engineered Adeno-Associated Virus Capsid Variants: Tropism Differences and
509 Mechanistic Insights. Viruses. 2024;16(3). Epub 20240312. doi: 10.3390/v16030442. PubMed PMID:
510 38543807; PubMed Central PMCID: PMCPMC10975205.
511 9. Muhuri M, Maeda Y, Ma H, Ram S, Fitzgerald KA, Tai PW, et al. Overcoming innate immune barriers
512 that impede AAV gene therapy vectors. J Clin Invest. 2021;131(1). doi: 10.1172/JCI143780. PubMed
513 PMID: 33393506; PubMed Central PMCID: PMCPMC7773343.
514 10. Rabinowitz J, Chan YK, Samulski RJ. Adeno-associated Virus (AAV) versus Immune Response.
515 Viruses. 2019;11(2). Epub 20190125. doi: 10.3390/v11020102. PubMed PMID: 30691064; PubMed
516 Central PMCID: PMCPMC6409805.
517 11. Scallan CD, Jiang H, Liu T, Patarroyo-White S, Sommer JM, Zhou S, et al. Human immunoglobulin
518 inhibits liver transduction by AAV vectors at low AAV2 neutralizing titers in SCID mice. Blood.
519 2006;107(5):1810-7. Epub 20051025. doi: 10.1182/blood-2005-08-3229. PubMed PMID: 16249376.
520 12. Boutin S, Monteilhet V, Veron P, Leborgne C, Benveniste O, Montus MF, et al. Prevalence of serum
521 IgG and neutralizing factors against adeno-associated virus (AAV) types 1, 2, 5, 6, 8, and 9 in the
522 healthy population: implications for gene therapy using AAV vectors. Hum Gene Ther.
523 2010;21(6):704-12. doi: 10.1089/hum.2009.182. PubMed PMID: 20095819.
524 13. Zaiss AK, Cotter MJ, White LR, Clark SA, Wong NC, Holers VM, et al. Complement is an essential
525 component of the immune response to adeno-associated virus vectors. J Virol. 2008;82(6):2727-40.
526 Epub 20080116. doi: 10.1128/JVI.01990-07. PubMed PMID: 18199646; PubMed Central PMCID:
527 PMCPMC2259003.

528 14. Arjomandnejad M, Sylvia K, Blackwood M, Nixon T, Tang Q, Muhuri M, et al. Modulating immune
529 responses to AAV by expanded polyclonal T-regs and capsid specific chimeric antigen receptor T-
530 regulatory cells. Mol Ther Methods Clin Dev. 2021;23:490-506. Epub 20211028. doi:
531 10.1016/j.omtm.2021.10.010. PubMed PMID: 34853797; PubMed Central PMCID:
532 PMCPMC8605179.
533 15. Basner-Tschakarjan E, Mingozzi F. Cell-Mediated Immunity to AAV Vectors, Evolving Concepts and
534 Potential Solutions. Front Immunol. 2014;5:350. Epub 20140723. doi: 10.3389/fimmu.2014.00350.
535 PubMed PMID: 25101090; PubMed Central PMCID: PMCPMC4107954.
536 16. Lehrer RI, Lu W. alpha-Defensins in human innate immunity. Immunol Rev. 2012;245(1):84-112.
537 Epub 2011/12/16. doi: 10.1111/j.1600-065X.2011.01082.x. PubMed PMID: 22168415.
538 17. Selsted ME, Ouellette AJ. Mammalian defensins in the antimicrobial immune response. Nat
539 Immunol. 2005;6(6):551-7. Epub 2005/05/24. doi: 10.1038/ni1206. PubMed PMID: 15908936.
540 18. Wilson SS, Wiens ME, Smith JG. Antiviral mechanisms of human defensins. J Mol Biol.
541 2013;425(24):4965-80. Epub 20131002. doi: 10.1016/j.jmb.2013.09.038. PubMed PMID: 24095897;
542 PubMed Central PMCID: PMCPMC3842434.
543 19. Holly MK, Diaz K, Smith JG. Defensins in Viral Infection and Pathogenesis. Annual review of virology.
544 2017;4(1):369-91. Epub 20170717. doi: 10.1146/annurev-virology-101416-041734. PubMed PMID:
545 28715972.
546 20. Rajabi M, Ericksen B, Wu X, de Leeuw E, Zhao L, Pazgier M, et al. Functional determinants of human
547 enteric alpha-defensin HD5: crucial role for hydrophobicity at dimer interface. J Biol Chem.
548 2012;287(26):21615-27. Epub 20120509. doi: 10.1074/jbc.M112.367995. PubMed PMID:
549 22573326; PubMed Central PMCID: PMCPMC3381126.

550 21. Gounder AP, Wiens ME, Wilson SS, Lu W, Smith JG. Critical determinants of human alpha-defensin
551 5 activity against non-enveloped viruses. J Biol Chem. 2012;287(29):24554-62. Epub 20120525. doi:
552 10.1074/jbc.M112.354068. PubMed PMID: 22637473; PubMed Central PMCID: PMCPMC3397880.
553 22. Porter JM, Oswald MS, Sharma A, Emmanuel S, Kansol A, Bennett A, et al. A Single Surface-Exposed
554 Amino Acid Determines Differential Neutralization of AAV1 and AAV6 by Human Alpha-Defensins. J
555 Virol. 2023;97(3):e0006023. Epub 20230314. doi: 10.1128/jvi.00060-23. PubMed PMID: 36916912;
556 PubMed Central PMCID: PMCPMC10062168.
557 23. Xu C, Wang A, Marin M, Honnen W, Ramasamy S, Porter E, et al. Human Defensins Inhibit SARS-
558 CoV-2 Infection by Blocking Viral Entry. Viruses. 2021;13(7). Epub 20210626. doi:
559 10.3390/v13071246. PubMed PMID: 34206990; PubMed Central PMCID: PMCPMC8310277.
560 24. Holly MK, Smith JG. Paneth Cells during Viral Infection and Pathogenesis. Viruses. 2018;10(5). Epub
561 20180426. doi: 10.3390/v10050225. PubMed PMID: 29701691; PubMed Central PMCID:
562 PMCPMC5977218.
563 25. Spencer JD, Hains DS, Porter E, Bevins CL, DiRosario J, Becknell B, et al. Human alpha defensin 5
564 expression in the human kidney and urinary tract. PLoS One. 2012;7(2):e31712. Epub 20120216.
565 doi: 10.1371/journal.pone.0031712. PubMed PMID: 22359618; PubMed Central PMCID:
566 PMCPMC3281003.
567 26. Brinkmann V, Reichard U, Goosmann C, Fauler B, Uhlemann Y, Weiss DS, et al. Neutrophil
568 extracellular traps kill bacteria. Science. 2004;303(5663):1532-5. doi: 10.1126/science.1092385.
569 PubMed PMID: 15001782.
570 27. Smith JG, Nemerow GR. Mechanism of adenovirus neutralization by Human alpha-defensins. Cell
571 host & microbe. 2008;3(1):11-9. Epub 2008/01/15. doi: 10.1016/j.chom.2007.12.001. PubMed
572 PMID: 18191790.

573 28. Smith JG, Silvestry M, Lindert S, Lu W, Nemerow GR, Stewart PL. Insight into the mechanisms of
574 adenovirus capsid disassembly from studies of defensin neutralization. PLoS Pathog.
575 2010;6(6):e1000959. Epub 20100624. doi: 10.1371/journal.ppat.1000959. PubMed PMID:
576 20585634; PubMed Central PMCID: PMCPMC2891831.
577 29. Wiens ME, Smith JG. Alpha-defensin HD5 inhibits furin cleavage of human papillomavirus 16 L2 to
578 block infection. J Virol. 2015;89(5):2866-74. Epub 20141224. doi: 10.1128/JVI.02901-14. PubMed
579 PMID: 25540379; PubMed Central PMCID: PMCPMC4325740.
580 30. Wiens ME, Smith JG. alpha-Defensin HD5 Inhibits Human Papillomavirus 16 Infection via Capsid
581 Stabilization and Redirection to the Lysosome. mBio. 2017;8(1). Epub 20170124. doi:
582 10.1128/mBio.02304-16. PubMed PMID: 28119475; PubMed Central PMCID: PMCPMC5263252.
583 31. Buck CB, Day PM, Thompson CD, Lubkowski J, Lu W, Lowy DR, et al. Human alpha-defensins block
584 papillomavirus infection. Proc Natl Acad Sci U S A. 2006;103(5):1516-21. Epub 20060123. doi:
585 10.1073/pnas.0508033103. PubMed PMID: 16432216; PubMed Central PMCID: PMCPMC1360544.
586 32. Dugan AS, Maginnis MS, Jordan JA, Gasparovic ML, Manley K, Page R, et al. Human alpha-defensins
587 inhibit BK virus infection by aggregating virions and blocking binding to host cells. J Biol Chem.
588 2008;283(45):31125-32. Epub 20080909. doi: 10.1074/jbc.M805902200. PubMed PMID: 18782756;
589 PubMed Central PMCID: PMCPMC2576552.
590 33. Zins SR, Nelson CD, Maginnis MS, Banerjee R, O'Hara BA, Atwood WJ. The human alpha defensin
591 HD5 neutralizes JC polyomavirus infection by reducing endoplasmic reticulum traffic and stabilizing
592 the viral capsid. J Virol. 2014;88(2):948-60. Epub 20131106. doi: 10.1128/JVI.02766-13. PubMed
593 PMID: 24198413; PubMed Central PMCID: PMCPMC3911681.
594 34. Hu CT, Diaz K, Yang LC, Sharma A, Greenberg HB, Smith JG. Corrected and republished from: "VP4
595 Is a Determinant of Alpha-Defensin Modulation of Rotaviral Infection". J Virol.

596 2023;97(10):e0096223. Epub 20231003. doi: 10.1128/jvi.00962-23. PubMed PMID: 37787534;
597 PubMed Central PMCID: PMCPMC10617384.
598 35. Virella-Lowell I, Poirier A, Chesnut KA, Brantly M, Flotte TR. Inhibition of recombinant adeno-
599 associated virus (rAAV) transduction by bronchial secretions from cystic fibrosis patients. Gene Ther.
600 2000;7(20):1783-9. doi: 10.1038/sj.gt.3301268. PubMed PMID: 11083501.
601 36. Diaz K, Hu CT, Sul Y, Bromme BA, Myers ND, Skorohodova KV, et al. Defensin-driven viral evolution.
602 PLoS Pathog. 2020;16(11):e1009018. Epub 20201124. doi: 10.1371/journal.ppat.1009018. PubMed
603 PMID: 33232373; PubMed Central PMCID: PMCPMC7723274.
604 37. Nguyen EK, Nemerow GR, Smith JG. Direct evidence from single-cell analysis that human alpha-
605 defensins block adenovirus uncoating to neutralize infection. J Virol. 2010;84(8):4041-9. Epub
606 20100203. doi: 10.1128/JVI.02471-09. PubMed PMID: 20130047; PubMed Central PMCID:
607 PMCPMC2849482.
608 38. Tenge VR, Gounder AP, Wiens ME, Lu W, Smith JG. Delineation of interfaces on human alpha-
609 defensins critical for human adenovirus and human papillomavirus inhibition. PLoS Pathog.
610 2014;10(9):e1004360. Epub 20140904. doi: 10.1371/journal.ppat.1004360. PubMed PMID:
611 25188351; PubMed Central PMCID: PMCPMC4154873.
612 39. Bartlett JS, Wilcher R, Samulski RJ. Infectious entry pathway of adeno-associated virus and adeno-
613 associated virus vectors. J Virol. 2000;74(6):2777-85. PubMed PMID: 10684294.
614 40. Girod A, Wobus CE, Zadori Z, Ried M, Leike K, Tijssen P, et al. The VP1 capsid protein of adeno-
615 associated virus type 2 is carrying a phospholipase A2 domain required for virus infectivity. J Gen
616 Virol. 2002;83(Pt 5):973-8. Epub 2002/04/19. doi: 10.1099/0022-1317-83-5-973. PubMed PMID:
617 11961250.
618 41. Kronenberg S, Bottcher B, von der Lieth CW, Bleker S, Kleinschmidt JA. A conformational change in
619 the adeno-associated virus type 2 capsid leads to the exposure of hidden VP1 N termini. J Virol.

620 2005;79(9):5296-303. Epub 2005/04/14. doi: 10.1128/JVI.79.9.5296-5303.2005. PubMed PMID:
621 15827144; PubMed Central PMCID: PMCPMC1082756.
622 42. Sonntag F, Bleker S, Leuchs B, Fischer R, Kleinschmidt JA. Adeno-associated virus type 2 capsids with
623 externalized VP1/VP2 trafficking domains are generated prior to passage through the cytoplasm
624 and are maintained until uncoating occurs in the nucleus. J Virol. 2006;80(22):11040-54. Epub
625 20060906. doi: 10.1128/JVI.01056-06. PubMed PMID: 16956943; PubMed Central PMCID:
626 PMCPMC1642181.
627 43. Stahnke S, Lux K, Uhrig S, Kreppel F, Hosel M, Coutelle O, et al. Intrinsic phospholipase A2 activity of
628 adeno-associated virus is involved in endosomal escape of incoming particles. Virology.
629 2011;409(1):77-83. Epub 20101025. doi: 10.1016/j.virol.2010.09.025. PubMed PMID: 20974479.
630 44. Wobus CE, Hugle-Dorr B, Girod A, Petersen G, Hallek M, Kleinschmidt JA. Monoclonal antibodies
631 against the adeno-associated virus type 2 (AAV-2) capsid: epitope mapping and identification of
632 capsid domains involved in AAV-2-cell interaction and neutralization of AAV-2 infection. J Virol.
633 2000;74(19):9281-93. Epub 2000/09/12. doi: 10.1128/jvi.74.19.9281-9293.2000. PubMed PMID:
634 10982375; PubMed Central PMCID: PMCPMC102127.
635 45. Wistuba A, Kern A, Weger S, Grimm D, Kleinschmidt JA. Subcellular compartmentalization of adeno-
636 associated virus type 2 assembly. J Virol. 1997;71(2):1341-52. doi: 10.1128/JVI.71.2.1341-
637 1352.1997. PubMed PMID: 8995658; PubMed Central PMCID: PMCPMC191189.
638 46. Salganik M, Venkatakrishnan B, Bennett A, Lins B, Yarbrough J, Muzyczka N, et al. Evidence for pH-
639 dependent protease activity in the adeno-associated virus capsid. J Virol. 2012;86(21):11877-85.
640 Epub 20120822. doi: 10.1128/JVI.01717-12. PubMed PMID: 22915820; PubMed Central PMCID:
641 PMCPMC3486322.
642 47. Rayaprolu V, Kruse S, Kant R, Venkatakrishnan B, Movahed N, Brooke D, et al. Comparative analysis
643 of adeno-associated virus capsid stability and dynamics. J Virol. 2013;87(24):13150-60. Epub

644 2013/09/27. doi: 10.1128/JVI.01415-13. PubMed PMID: 24067976; PubMed Central PMCID:
645 PMCPMC3838259.
646 48. Lins-Austin B, Patel S, Mietzsch M, Brooke D, Bennett A, Venkatakrishnan B, et al. Adeno-Associated
647 Virus (AAV) Capsid Stability and Liposome Remodeling During Endo/Lysosomal pH Trafficking.
648 Viruses. 2020;12(6). Epub 2020/06/25. doi: 10.3390/v12060668. PubMed PMID: 32575696;
649 PubMed Central PMCID: PMCPMC7354436.
650 49. Grieger JC, Snowdy S, Samulski RJ. Separate basic region motifs within the adeno-associated virus
651 capsid proteins are essential for infectivity and assembly. J Virol. 2006;80(11):5199-210. Epub
652 2006/05/16. doi: 10.1128/JVI.02723-05. PubMed PMID: 16699000; PubMed Central PMCID:
653 PMCPMC1472161.
654 50. Summerford C, Samulski RJ. Membrane-associated heparan sulfate proteoglycan is a receptor for
655 adeno-associated virus type 2 virions. J Virol. 1998;72(2):1438-45. Epub 1998/01/28. PubMed PMID:
656 9445046; PubMed Central PMCID: PMCPMC124624.
657 51. Zengel J, Carette JE. Structural and cellular biology of adeno-associated virus attachment and entry.
658 Adv Virus Res. 2020;106:39-84. Epub 20200213. doi: 10.1016/bs.aivir.2020.01.002. PubMed PMID:
659 32327148.
660 52. Dudek AM, Pillay S, Puschnik AS, Nagamine CM, Cheng F, Qiu J, et al. An Alternate Route for Adeno-
661 associated Virus (AAV) Entry Independent of AAV Receptor. J Virol. 2018;92(7). Epub 2018/01/19.
662 doi: 10.1128/JVI.02213-17. PubMed PMID: 29343568; PubMed Central PMCID: PMCPMC5972900.
663 53. Pillay S, Meyer NL, Puschnik AS, Davulcu O, Diep J, Ishikawa Y, et al. An essential receptor for adeno-
664 associated virus infection. Nature. 2016;530(7588):108-12. Epub 20160127. doi:
665 10.1038/nature16465. PubMed PMID: 26814968; PubMed Central PMCID: PMCPMC4962915.

666 54. Dudek AM, Zabaleta N, Zinn E, Pillay S, Zengel J, Porter C, et al. GPR108 Is a Highly Conserved AAV
667 Entry Factor. Mol Ther. 2020;28(2):367-81. Epub 20191113. doi: 10.1016/j.ymthe.2019.11.005.
668 PubMed PMID: 31784416; PubMed Central PMCID: PMCPMC7000996.
669 55. Meisen WH, Nejad ZB, Hardy M, Zhao H, Oliverio O, Wang S, et al. Pooled Screens Identify GPR108
670 and TM9SF2 as Host Cell Factors Critical for AAV Transduction. Mol Ther Methods Clin Dev.
671 2020;17:601-11. Epub 20200317. doi: 10.1016/j.omtm.2020.03.012. PubMed PMID: 32280726;
672 PubMed Central PMCID: PMCPMC7139131.
673 56. Mantyla E, Kann M, Vihinen-Ranta M. Protoparvovirus Knocking at the Nuclear Door. Viruses.
674 2017;9(10). Epub 20171002. doi: 10.3390/v9100286. PubMed PMID: 28974036; PubMed Central
675 PMCID: PMCPMC5691637.
676 57. Sanlioglu S, Benson PK, Yang J, Atkinson EM, Reynolds T, Engelhardt JF. Endocytosis and nuclear
677 trafficking of adeno-associated virus type 2 are controlled by rac1 and phosphatidylinositol-3 kinase
678 activation. J Virol. 2000;74(19):9184-96. doi: 10.1128/jvi.74.19.9184-9196.2000. PubMed PMID:
679 10982365; PubMed Central PMCID: PMCPMC102117.
680 58. Xiao PJ, Samulski RJ. Cytoplasmic trafficking, endosomal escape, and perinuclear accumulation of
681 adeno-associated virus type 2 particles are facilitated by microtubule network. J Virol.
682 2012;86(19):10462-73. Epub 20120718. doi: 10.1128/JVI.00935-12. PubMed PMID: 22811523;
683 PubMed Central PMCID: PMCPMC3457265.
684 59. Sutter SO, Lkharrazi A, Schraner EM, Michaelsen K, Meier AF, Marx J, et al. Adeno-associated virus
685 type 2 (AAV2) uncoating is a stepwise process and is linked to structural reorganization of the
686 nucleolus. PLoS Pathog. 2022;18(7):e1010187. Epub 20220711. doi: 10.1371/journal.ppat.1010187.
687 PubMed PMID: 35816507; PubMed Central PMCID: PMCPMC9302821.

688 60. Johnson JS, Samulski RJ. Enhancement of adeno-associated virus infection by mobilizing capsids into
689 and out of the nucleolus. J Virol. 2009;83(6):2632-44. Epub 20081224. doi: 10.1128/JVI.02309-08.
690 PubMed PMID: 19109385; PubMed Central PMCID: PMCPMC2648275.
691 61. Venkatakrishnan B, Yarbrough J, Domsic J, Bennett A, Bothner B, Kozyreva OG, et al. Structure and
692 dynamics of adeno-associated virus serotype 1 VP1-unique N-terminal domain and its role in capsid
693 trafficking. J Virol. 2013;87(9):4974-84. Epub 20130220. doi: 10.1128/JVI.02524-12. PubMed PMID:
694 23427155; PubMed Central PMCID: PMCPMC3624325.
695 62. Bleker S, Sonntag F, Kleinschmidt JA. Mutational analysis of narrow pores at the fivefold symmetry
696 axes of adeno-associated virus type 2 capsids reveals a dual role in genome packaging and activation
697 of phospholipase A2 activity. J Virol. 2005;79(4):2528-40. doi: 10.1128/JVI.79.4.2528-2540.2005.
698 PubMed PMID: 15681453; PubMed Central PMCID: PMCPMC546590.
699 63. Horowitz ED, Finn MG, Asokan A. Tyrosine cross-linking reveals interfacial dynamics in adeno-
700 associated viral capsids during infection. ACS Chem Biol. 2012;7(6):1059-66. Epub 20120406. doi:
701 10.1021/cb3000265. PubMed PMID: 22458529; PubMed Central PMCID: PMCPMC3376196.
702 64. Emmanuel SN, Smith JK, Hsi J, Tseng YS, Kaplan M, Mietzsch M, et al. Structurally Mapping Antigenic
703 Epitopes of Adeno-associated Virus 9: Development of Antibody Escape Variants. J Virol.
704 2022;96(3):e0125121. Epub 20211110. doi: 10.1128/JVI.01251-21. PubMed PMID: 34757842;
705 PubMed Central PMCID: PMCPMC8827038.
706 65. Havlik LP, Simon KE, Smith JK, Klinc KA, Tse LV, Oh DK, et al. Coevolution of Adeno-associated Virus
707 Capsid Antigenicity and Tropism through a Structure-Guided Approach. J Virol. 2020;94(19). Epub
708 20200915. doi: 10.1128/JVI.00976-20. PubMed PMID: 32669336; PubMed Central PMCID:
709 PMCPMC7495376.
710 66. Mietzsch M, Smith JK, Yu JC, Banala V, Emmanuel SN, Jose A, et al. Characterization of AAV-Specific
711 Affinity Ligands: Consequences for Vector Purification and Development Strategies. Mol Ther

712 Methods Clin Dev. 2020;19:362-73. Epub 20201004. doi: 10.1016/j.omtm.2020.10.001. PubMed
713 PMID: 33145372; PubMed Central PMCID: PMCPMC7591348.
714 67. Douar AM, Poulard K, Stockholm D, Danos O. Intracellular trafficking of adeno-associated virus
715 vectors: routing to the late endosomal compartment and proteasome degradation. J Virol.
716 2001;75(4):1824-33. PubMed PMID: 11160681.
717 68. Hansen J, Qing K, Srivastava A. Adeno-associated virus type 2-mediated gene transfer: altered
718 endocytic processing enhances transduction efficiency in murine fibroblasts. J Virol.
719 2001;75(9):4080-90. doi: 10.1128/JVI.75.9.4080-4090.2001. PubMed PMID: 11287557; PubMed
720 Central PMCID: PMCPMC114153.
721 69. Zhao C, Porter JM, Burke PC, Arnberg N, Smith JG. Alpha-defensin binding expands human
722 adenovirus tropism. PLoS Pathog. 2024;20(6):e1012317. Epub 20240620. doi:
723 10.1371/journal.ppat.1012317. PubMed PMID: 38900833; PubMed Central PMCID:
724 PMCPMC11230588.
725 70. Wilson SS, Bromme BA, Holly MK, Wiens ME, Gounder AP, Sul Y, et al. Alpha-defensin-dependent
726 enhancement of enteric viral infection. PLoS Pathog. 2017;13(6):e1006446. Epub 20170616. doi:
727 10.1371/journal.ppat.1006446. PubMed PMID: 28622386; PubMed Central PMCID:
728 PMCPMC5489213.
729 71. Rapista A, Ding J, Benito B, Lo YT, Neiditch MB, Lu W, et al. Human defensins 5 and 6 enhance HIV-
730 1 infectivity through promoting HIV attachment. Retrovirology. 2011;8:45. Epub 20110614. doi:
731 10.1186/1742-4690-8-45. PubMed PMID: 21672195; PubMed Central PMCID: PMCPMC3146398.
732 72. Hazlett L, Wu M. Defensins in innate immunity. Cell Tissue Res. 2011;343(1):175-88. Epub
733 20100821. doi: 10.1007/s00441-010-1022-4. PubMed PMID: 20730446.
734 73. Yan Z, Zak R, Zhang Y, Ding W, Godwin S, Munson K, et al. Distinct classes of proteasome-modulating
735 agents cooperatively augment recombinant adeno-associated virus type 2 and type 5-mediated

736 transduction from the apical surfaces of human airway epithelia. J Virol. 2004;78(6):2863-74. doi:
737 10.1128/jvi.78.6.2863-2874.2004. PubMed PMID: 14990705; PubMed Central PMCID:
738 PMCPMC353734.
739 74. Wu Z, Asokan A, Grieger JC, Govindasamy L, Agbandje-McKenna M, Samulski RJ. Single amino acid
740 changes can influence titer, heparin binding, and tissue tropism in different adeno-associated virus
741 serotypes. J Virol. 2006;80(22):11393-7. Epub 20060830. doi: 10.1128/JVI.01288-06. PubMed PMID:
742 16943302; PubMed Central PMCID: PMCPMC1642158.
743 75. Wu Z, Miller E, Agbandje-McKenna M, Samulski RJ. Alpha2,3 and alpha2,6 N-linked sialic acids
744 facilitate efficient binding and transduction by adeno-associated virus types 1 and 6. J Virol.
745 2006;80(18):9093-103. Epub 2006/08/31. doi: 10.1128/JVI.00895-06. PubMed PMID: 16940521;
746 PubMed Central PMCID: PMCPMC1563919.
747 76. Rabinowitz JE, Rolling F, Li C, Conrath H, Xiao W, Xiao X, et al. Cross-packaging of a single adeno-
748 associated virus (AAV) type 2 vector genome into multiple AAV serotypes enables transduction with
749 broad specificity. J Virol. 2002;76(2):791-801. doi: 10.1128/jvi.76.2.791-801.2002. PubMed PMID:
750 11752169; PubMed Central PMCID: PMCPMC136844.
751 77. Burger C, Gorbatyuk OS, Velardo MJ, Peden CS, Williams P, Zolotukhin S, et al. Recombinant AAV
752 viral vectors pseudotyped with viral capsids from serotypes 1, 2, and 5 display differential efficiency
753 and cell tropism after delivery to different regions of the central nervous system. Mol Ther.
754 2004;10(2):302-17. doi: 10.1016/j.ymthe.2004.05.024. PubMed PMID: 15294177.
755 78. Xiao X, Li J, Samulski RJ. Production of high-titer recombinant adeno-associated virus vectors in the
756 absence of helper adenovirus. J Virol. 1998;72(3):2224-32. doi: 10.1128/JVI.72.3.2224-2232.1998.
757 PubMed PMID: 9499080; PubMed Central PMCID: PMCPMC109519.
758 79. Bennett A, Patel S, Mietzsch M, Jose A, Lins-Austin B, Yu JC, et al. Thermal Stability as a Determinant
759 of AAV Serotype Identity. Mol Ther Methods Clin Dev. 2017;6:171-82. Epub 20170724. doi:

760 10.1016/j.omtm.2017.07.003. PubMed PMID: 28828392; PubMed Central PMCID:
761 PMCPMC5552060.
762 80. Pachitariu M, Stringer C. Cellpose 2.0: how to train your own model. Nat Methods.
763 2022;19(12):1634-41. Epub 20221107. doi: 10.1038/s41592-022-01663-4. PubMed PMID:
764 36344832; PubMed Central PMCID: PMCPMC9718665.
765 81. Stirling DR, Swain-Bowden MJ, Lucas AM, Carpenter AE, Cimini BA, Goodman A. CellProfiler 4:
766 improvements in speed, utility and usability. BMC Bioinformatics. 2021;22(1):433. Epub 20210910.
767 doi: 10.1186/s12859-021-04344-9. PubMed PMID: 34507520; PubMed Central PMCID:
768 PMCPMC8431850.

769

770

771 **Figure Legends**

772 **Figure 1. Both HD5 and HNP1 bind to AAV2 and neutralize infection.** Infection of AAV2 in the
773 presence of (A) HD5 or (B) HNP1. AAV2 was incubated with each defensin on ice prior to addition
774 to HeLa cells. Data are normalized to control infection in the absence of defensin and are the
775 mean ± SD of a minimum of 3 independent experiments. Mean IC_{50} values are indicated. Both
776 (C) HD5 and (D) HNP1 bind to AAV2. Background-corrected SPR sensorgrams are shown from
777 a concentration series of defensin interacting with immobilized AAV2. Colors correspond to
778 analyte (defensin) concentration, as indicated. Sensorgrams are representative of 2 independent
779 replicates for each defensin. Mean K_D values ± SD are indicated.

780 **Figure 2. HD5, but not HNP1, inhibits AAV2 binding to cells, while both defensins impose**
781 **a post-attachment block to infection.** Effects of (A) HD5 and (B) HNP1 on AAV2 binding to
782 HeLa cells. AAV2 was exposed to each defensin on ice prior to and during HeLa cell binding,
783 which was then quantified by qPCR. Data are normalized to the amount of virus bound in the
784 absence of defensin and are the mean ± SD of at least 3 independent experiments. The mean
785 HD5 IC_{50} value is indicated. Both (C) HD5 and (D) HNP1 inhibit AAV2 infection when added after
786 attachment of AAV2 to cells. Data are normalized to control infection in the absence of defensin
787 and are the mean ± SD of a minimum of 3 independent experiments. Mean IC_{50} values are
788 indicated.

789 **Figure 3. Both HD5 and HNP1 block VP1u exposure.** (A) Representative western blots of
790 AAV2 that was sequentially immunoprecipitated at 6 h p.i. first with the A1 (VP1u-specific)
791 antibody (top) then the A20 (intact capsid) antibody (bottom). Cells were infected in the presence
792 of 25 μM HD5, 25 μM HD5abu (ABU), or no defensin (ND). Uninfected cells (no virus, NV) were
793 included as a control. Blots were probed with the B1 antibody, and (B) the ratio of VP3 in the two
794 blots was quantified. (C) Representative western blots and (D) quantification of similar
795 experiments using 30 μM HNP1. (E) Representative western blots and (F) quantification of control

796 experiments where no defensin was present at the time of infection, but 30 μM HNP1 or no
797 defensin (ND) was added to the cell lysate prior to immunoprecipitation. (G and H) Representative
798 images and (I) quantification of HeLa cells in 96-well plates infected with AAV2 in the presence
799 or absence of the same concentrations of defensins that were used for immunoprecipitation.
800 Images were obtained 48 h p.i. at a resolution of 50 μm, and grayscale intensity correlates with
801 eGFP expression. Note that the infections were performed in parallel with the immunoprecipitation
802 experiments but that the HNP1 infection experiments were done separately from those with HD5
803 and HD5abu. For B, D, F, and I, each point is a biological replicate (n = 3), and bars are the mean
804 ± SD.

805 **Figure 4. HD5 and HNP1 block proteolytic cleavage of the capsid but do not alter capsid**
806 **thermostability.** Representative blots from additional replicates of the A20 immunoprecipitation
807 experiments from Fig 3A and 3C probed with the B1 antibody. Arrows mark a B1-reactive
808 proteolytic fragment of the capsid proteins that is detectable in (A) the presence of 25 μM HD5abu
809 (ABU) but not 25 μM HD5 and (B) the absence (ND) but not presence of 30 μM HNP1. (C) The
810 melting temperature (T_m) of AAV2 in the presence or absence of 25 μM HD5, 30 μM HNP1, or no
811 defensin at the indicated pHs. Each point is a biological replicate (n = 3), and bars are the mean
812 ± SD.

813 **Figure 5. Both HD5 and HNP1 inhibit AAV2 nuclear localization.** (A-C) The fraction of DyLight
814 488 (DL488)-labelled AAV2 in the nucleus of HeLa cells infected in the presence of 25 μM HD5
815 or 30 μM HNP1 was assessed 24 h p.i. by confocal microscopy and automated image analysis.
816 Control cells infected in the absence of defensin (ND) were analyzed immediately after cold
817 synchronization (0 h p.i.) or at 24 h p.i. (A) Scatter plots with a minimum of 35 cells per condition
818 are shown. Each replicate is shown separately and indicated by both symbol (Replicate 1 =
819 circles, 2 = squares, 3 = triangles, 4 = upside-down triangles) and color shade. n.d. = not done.
820 (B) Replicates from A were pooled and re-analyzed in aggregate for each condition. C)

821 Representative images of single cells from the experiments in A. Merged images include DAPI
822 (blue) and AAV2-DL488 (green). The fraction of DL488 signal in the nucleus is indicated for each
823 merged image. (D) Representative images of single cells from the experiments in A are shown to
824 depict the perinuclear region, located between the concentric yellow rings, which was used for
825 the analysis in E. The fraction of DL488 signal in the nucleus (n) and perinuclear region (p) is
826 indicated for each image. (E) The integrated intensity of the DL488 signal in the nucleus was
827 divided by that of the perinuclear region, and the log of this ratio is graphed. (F) The total cellular
828 integrated intensity of the DL488 signal was quantified. In all graphs, horizontal bars indicate
829 means. In B, E, and F, the shape and color of each data point corresponds to the replicates and
830 conditions in A. In C and D, scale bars indicate 10 μm, the DL488 signal was individually adjusted
831 for display purposes, and cells are from different replicates across conditions.

832 **Figure 6. Model of AAV neutralization by defensins.** Model of AAV2 infection in the absence
833 (left) and presence (right) of neutralizing concentrations of HD5 or HNP1. Host factors including
834 heparan sulfate proteoglycans (HSPG), the AAV receptor (AAVR), and GPR108 are depicted.
835 The red “x” indicates the block to cell binding upon pre-attachment exposure of AAV2 to HD5.
836 HNP1 is used to illustrate the effects of the intracellular defensin block, which is common to HD5
837 and HNP1. Figure created with BioRender.com.

838

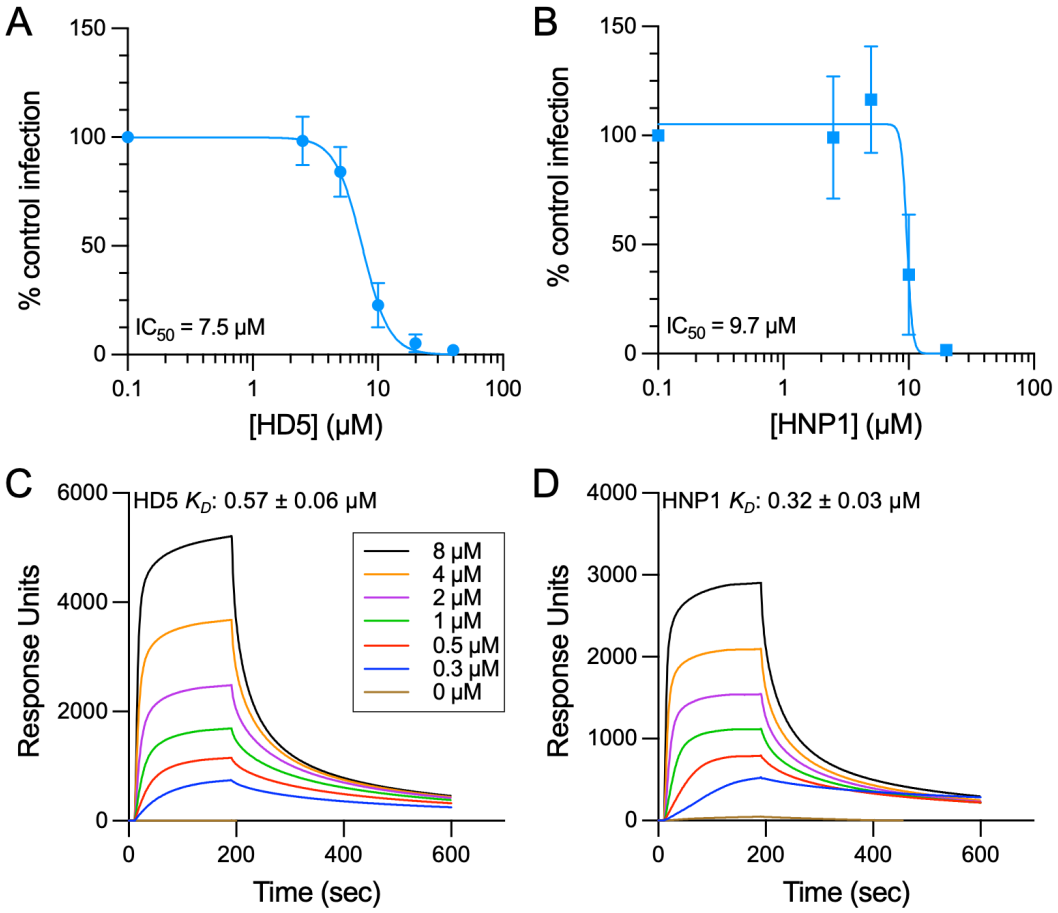

Figure 1. Both HD5 and HNP1 bind to AAV2 and neutralize infection. Infection of AAV2 in the presence of (A) HD5 or (B) HNP1. AAV2 was incubated with each defensin on ice prior to addition to HeLa cells. Data are normalized to control infection in the absence of defensin and are the mean ± SD of a minimum of 3 independent experiments. Mean IC_{50} values are indicated. Both (C) HD5 and (D) HNP1 bind to AAV2. Background-corrected SPR sensorgrams are shown from a concentration series of defensin interacting with immobilized AAV2. Colors correspond to analyte (defensin) concentration, as indicated. Sensorgrams are representative of 2 independent replicates for each defensin. Mean K_D values ± SD are indicated.

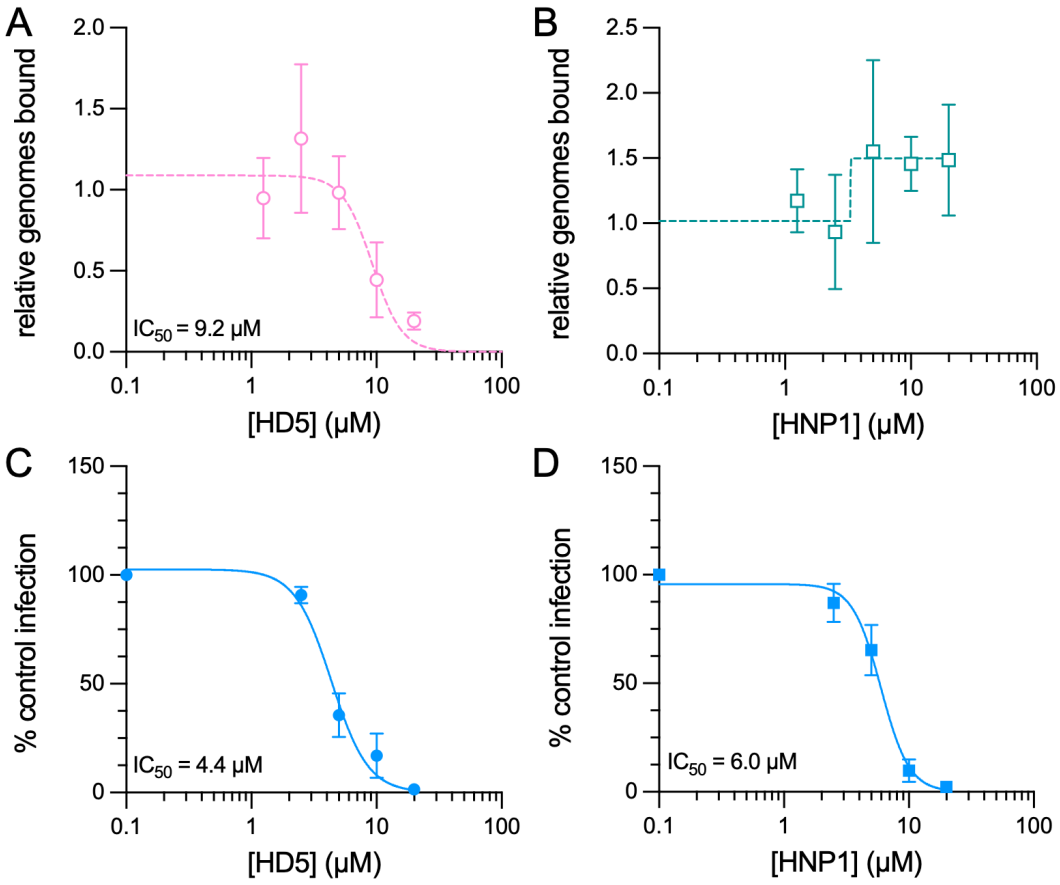

Figure 2. HD5, but not HNP1, inhibits AAV2 binding to cells, while both defensins impose a post-attachment block to infection. Effects of (A) HD5 and (B) HNP1 on AAV2 binding to HeLa cells. AAV2 was exposed to each defensin on ice prior to and during HeLa cell binding, which was then quantified by qPCR. Data are normalized to the amount of virus bound in the absence of defensin and are the mean ± SD of at least 3 independent experiments. The mean HD5 IC_{50} value is indicated. Both (C) HD5 and (D) HNP1 inhibit AAV2 infection when added after attachment of AAV2 to cells. Data are normalized to control infection in the absence of defensin and are the mean ± SD of a minimum of 3 independent experiments. Mean IC_{50} values are indicated.

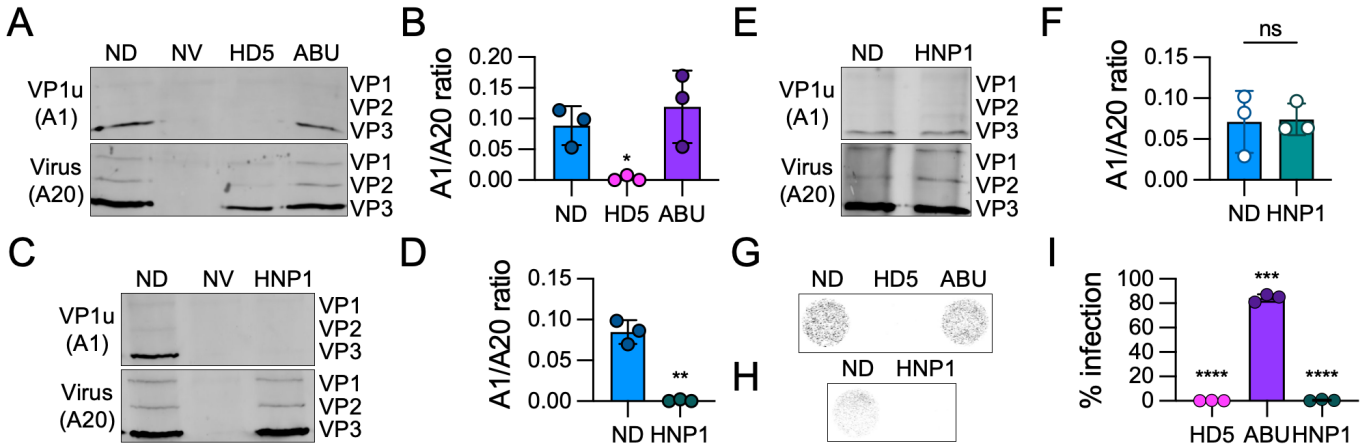

Figure 3. Both HD5 and HNP1 block VP1u exposure. (A) Representative western blots of AAV2 that was sequentially immunoprecipitated at 6 h p.i. first with the A1 (VP1u-specific) antibody (top) then the A20 (intact capsid) antibody (bottom). Cells were infected in the presence of 25 μM HD5, 25 μM HD5abu (ABU), or no defensin (ND). Uninfected cells (no virus, NV) were included as a control. Blots were probed with the B1 antibody, and (B) the ratio of VP3 in the two blots was quantified. (C) Representative western blots and (D) quantification of similar experiments using 30 μM HNP1. (E) Representative western blots and (F) quantification of control experiments where no defensin was present at the time of infection, but 30 μM HNP1 or no defensin (ND) was added to the cell lysate prior to immunoprecipitation. (G and H) Representative images and (I) quantification of HeLa cells in 96-well plates infected with AAV2 in the presence or absence of the same concentrations of defensins that were used for immunoprecipitation. Images were obtained 48 h p.i. at a resolution of 50 μm, and grayscale intensity correlates with eGFP expression. Note that the infections were performed in parallel with the immunoprecipitation experiments but that the HNP1 infection experiments were done separately from those with HD5 and HD5abu. For B, D, F, and I, each point is a biological replicate (n = 3), and bars are the mean ± SD.

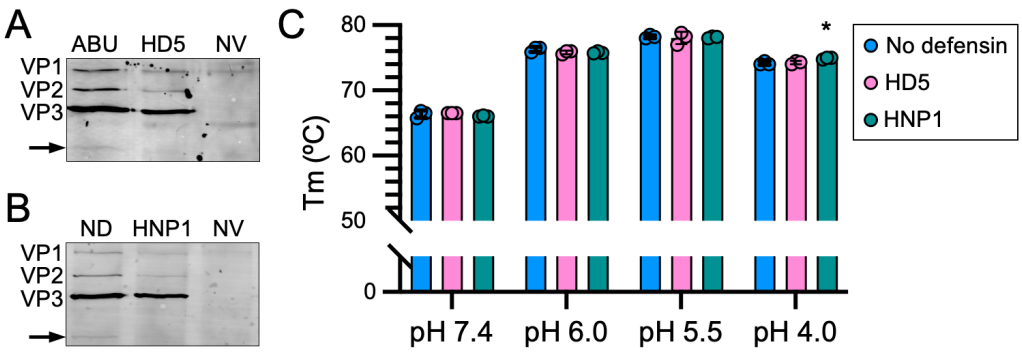

Figure 4. HD5 and HNP1 block proteolytic cleavage of the capsid but do not alter capsid thermostability. Representative blots from additional replicates of the A20 immunoprecipitation experiments from Fig 3A and 3C probed with the B1 antibody. Arrows mark a B1-reactive proteolytic fragment of the capsid proteins that is detectable in (A) the presence of 25 μM HD5abu (ABU) but not 25 μM HD5 and (B) the absence (ND) but not presence of 30 μM HNP1. (C) The melting temperature (T_m) of AAV2 in the presence or absence of 25 μM HD5, 30 μM HNP1, or no defensin at the indicated pHs. Each point is a biological replicate (n = 3), and bars are the mean ± SD.

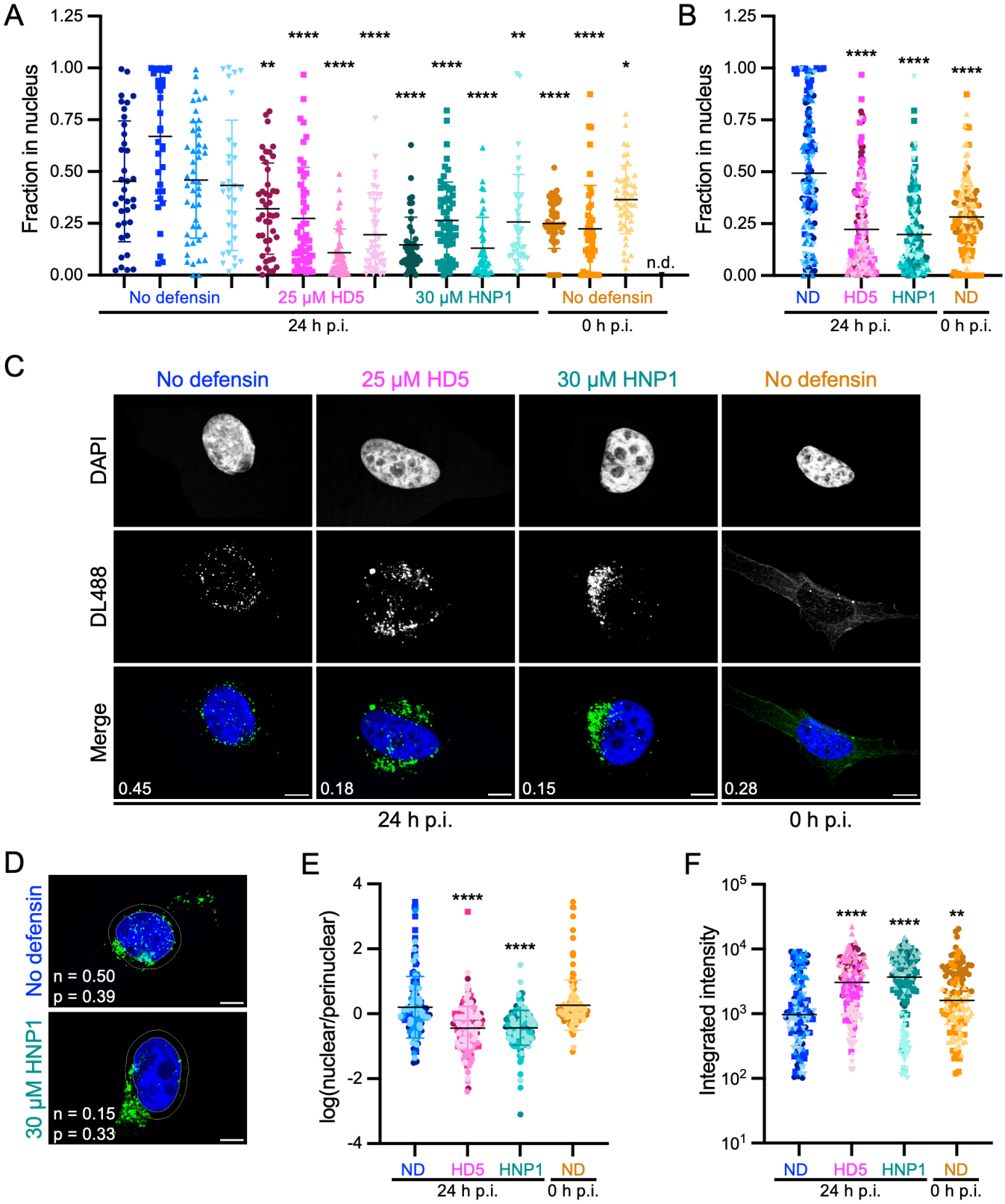
A
Fraction in nucleus
1.25
1.00
0.75
0.50
0.25
0.00
**
****
****
****
****
****
**
****
****
*
n.d.
No defensin
25 µM HD5
30 µM HNP1
No defensin
24 h p.i.
0 h p.i.
B
Fraction in nucleus
****
****
****
ND
HD5
HNP1
ND
24 h p.i.
0 h p.i.
C
No defensin
25 µM HD5
30 µM HNP1
No defensin
DAPI
DL488
Merge
0.45
0.18
0.15
0.28
24 h p.i.
0 h p.i.
D
No defensin
n = 0.50
p = 0.39
30 µM HNP1
n = 0.15
p = 0.33
E
log(nuclear/perinuclear)
4
2
0
-2
-4
****
****
ND
HD5
HNP1
ND
24 h p.i.
0 h p.i.
F
Integrated intensity
10^5
10^4
10^3
10^2
10^1
****
****
**
ND
HD5
HNP1
ND
24 h p.i.
0 h p.i.

Figure 5. Both HD5 and HNP1 inhibit AAV2 nuclear localization. (A-C) The fraction of DyLight 488 (DL488)-labelled AAV2 in the nucleus of HeLa cells infected in the presence of 25 μM HD5 or 30 μM HNP1 was assessed 24 h p.i. by confocal microscopy and automated image analysis. Control cells infected in the absence of defensin (ND) were analyzed immediately after cold synchronization (0 h p.i.) or at 24 h p.i. (A) Scatter plots with a minimum of 35 cells per condition are shown. Each replicate is shown separately and indicated by both symbol (Replicate 1 = circles, 2 = squares, 3 = triangles, 4 = upside-down triangles) and color shade. n.d. = not done. (B) Replicates from A were pooled and re-analyzed in aggregate for each condition. C) Representative images of single cells from the experiments in A. Merged images include DAPI (blue) and AAV2-DL488 (green). The fraction of DL488 signal in the nucleus is indicated for each merged image. (D) Representative images of single cells from the experiments in A are shown to depict the perinuclear region, located between the concentric yellow rings, which was used for the analysis in E. The fraction of DL488 signal in the nucleus (n) and perinuclear region (p) is indicated for each image. (E) The integrated intensity of the DL488 signal in the nucleus was divided by that of the perinuclear region, and the log of this ratio is graphed. (F) The total cellular integrated intensity of the DL488 signal was quantified. In all graphs, horizontal bars indicate means. In B, E, and F, the shape and color of each data point corresponds to the replicates and conditions in A. In C and D, scale bars indicate 10 μm, the DL488 signal was individually adjusted for display purposes, and cells are from different replicates across conditions.

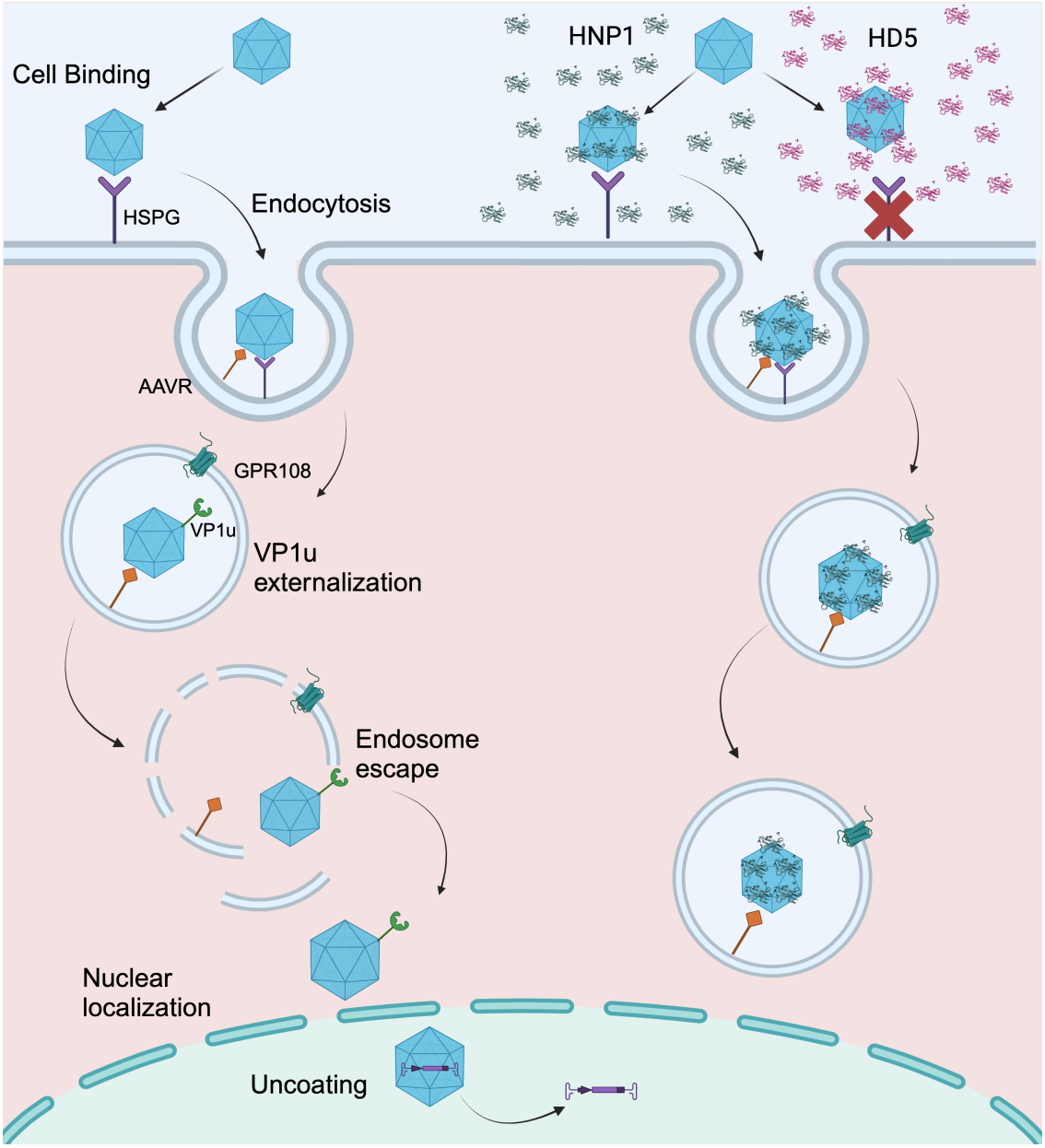

Figure 6. Model of AAV neutralization by defensins. Model of AAV2 infection in the absence (left) and presence (right) of neutralizing concentrations of HD5 or HNP1. Host factors including heparan sulfate proteoglycans (HSPG), the AAV receptor (AAVR), and GPR108 are depicted. The red "x" indicates the block to cell binding upon pre-attachment exposure of AAV2 to HD5. HNP1 is used to illustrate the effects of the intracellular defensin block, which is common to HD5 and HNP1. Figure created with BioRender.com.